Journal of Catalysis 392 (2020) 56–68

Contents lists available at ScienceDirect

Journal of Catalysis

journal homepage: www.elsevier.com/locate/jcat

Catalysis of oxygen reduction reaction for H_2O_2 electrogeneration: The impact of different conductive carbon matrices and their physicochemical properties

Paulo Jorge Marques Cordeiro-Junior [a,*], Matheus Schiavon Kronka [a,b], Lorena Athie Goulart [a], Nathalia Carolina Veríssimo [c], Lucia Helena Mascaro [d], Mauro Coelho dos Santos [e], Rodnei Bertazzoli [c,f], Marcos Roberto de Vasconcelos Lanza [a,b,*]

[a] São Carlos Institute of Chemistry (IQSC), University of São Paulo (USP), Avenida Trabalhador São-carlense 400, São Carlos, SP 13566-590, Brazil
[b] National Institute of Alternative Technologies for Detection, Toxicological Evaluation and Removal of Micropollutants and Radioactive Substances (INCT-DATREM), Institute of Chemistry, São Paulo State University, Araraquara, São Paulo, Brazil
[c] Faculty of Mechanical Engineering, State University of Campinas (Unicamp), Rua Mendeleyev 200, Campinas, SP 13083-860, Brazil
[d] Department of Chemistry, Federal University of São Carlos (UFSCar), Rodovia Washington Luiz km 235, São Carlos, SP 13565-905, Brazil
[e] Laboratório de Eletroquímica e Materiais Nanoestruturados (LEMN), Centro de Ciências Naturais e Humanas (CCNH), Federal University of ABC (UFABC), Rua Santa Adélia 166, Santo André, SP 09210-170, Brazil
[f] Brazilian Water Research Center- BWRC, University of Campinas, 13083-970, Campinas- SP, Brazil

ARTICLE INFO

Article history:
Received 19 May 2020
Revised 1 September 2020
Accepted 21 September 2020
Available online 7 October 2020

Keywords:
Carbon-based materials
Oxygen reduction reaction
Hydrogen peroxide electrosynthesis
Structural and electrochemical characterization

ABSTRACT

Carbon-based catalysts are widely used in oxygen reduction reactions (ORR) via 2e- for H_2O_2 electrogeneration. The direct comparability of the structural proprieties of different carbon matrices applied on ORR, however, has never been tested. Here, we evaluate how the electrochemical and structural properties of different carbon-based materials, including carbon Printex XE2B (PXE2BC), Printex L6 (PL6C), carbon derived from lignin (LIGC), graphite (GRA) and glassy carbon (GC), affect on ORR. All the materials were characterized by Raman spectroscopy, X-ray photoelectron spectrometry (XPS), elementary analysis, field emission gun scanning electron microscopy, surface area measurements and electrochemical assays for the evaluation of ORR. Notably, the morphology, the size of the particles and the types of functional groups present in the structure of carbon materials were keys in the efficiency of ORR. The carbon materials PL6C and PXE2BC with high surface area and oxygenated functional groups in their structure displaced the ORR potential, facilitating the reaction. Carbon materials with less surface area, such as GRA, LIGC and GC, and whose main functional groups in their structures were non-oxygenated or nitrogenated, were less active in ORR. The displacement of the potential and the efficiency of H_2O_2 generation were directly dependent on the electrochemical and structural characteristics of the materials used as catalysts. These results are particularly relevant regarding a proper choice of carbon catalyst can increase the efficiency of ORR.

1. Introduction

Hydrogen peroxide (H_2O_2) is considered one of the most powerful oxidizing agents; and due to its remarkable properties, this chemical compound is used as an important reagent in several applications, including tissue bleaching [1,2] and organic and inorganic syntheses [3,4]. H_2O_2 is commonly used in the treatment of wastewater via advanced oxidation processes (AOP) [5,6]. The advanced oxidation technique involves the use of H_2O_2 as a precursor of hydroxyl radical, and this explains the reason why the technique is regarded a green process, since the treatment reaction leads to the formation of inoculum products (such as CO_2, H_2O and inorganic compounds). When total mineralization fails to be reached, the by-products formed in the process exhibit lower toxicity compared to the initial products subjected to degradation.

H_2O_2 is commonly synthesized via anthraquinone oxidation process as described by Kirchner [7]; this process involves the initial reduction of anthraquinone organic compound to corresponding hydroanthraquinone by H_2. The reduced species are then oxidized in the presence of O_2, regenerating the initial compound

* Corresponding authors.
E-mail addresses: pjmcjunior@usp.br (P.J.M. Cordeiro-Junior), marcoslanza@usp.br (Marcos Roberto de Vasconcelos Lanza).

https://doi.org/10.1016/j.jcat.2020.09.020
0021-9517/

and H_2O_2. This synthesis process has been shown to present some disadvantages. Among these disadvantages include the use and recovery of metal catalysts, systems subjected to high temperature and pressure, and the use of organic solvents for the purification of the H_2O_2 generated [7,8].

An alternative process to H_2O_2 synthesis is oxygen reduction reaction (ORR), which involves the reduction of molecular oxygen on the cathode surface via 2 electrons (Eq. (1)). This electrochemical reaction is complex, once H_2O_2 can be reduced again via 2 more electrons forming H_2O (Eq. (2)), while molecular O_2 can be reduced directly to H_2O via 4 electrons (Eq. (3)) [8–12].

$$O_2 + 4H^+ + 4e^- \rightarrow 2H_2O \quad (1)$$

$$H_2O_2 + 2H^+ + 2e^- \rightarrow 2H_2O \quad (2)$$

$$O_2 + 2H^+ + 2e^- \rightarrow H_2O_2 \quad (3)$$

The advantages of ORR mechanism for H_2O_2 generation are: 1) it does not involve the use of hazardous reagents; 2) H_2O_2 purification is not required; and 3) it uses a green reagent – the electron. Furthermore, the ORR process allows the *in situ* electrogeneration of H_2O_2, thus avoiding the need for transport and storage of the reagent [8].

In the past few years, there has been considerable interest in the development of cathode material which is directly related to the system efficiency in ORR for H_2O_2 electrosynthesis, as shown in different works published in the literature [8,13–16]. The development of the cathode material components should take into account the binding energy of the intermediate species generated (•OOH), which must have an intermediate interaction with the electrode catalytic surface to generate H_2O_2. Once there is a strong interaction, the •OOH generated remains adsorbed for a longer period, and this increases the possibility of another reduction reaction, forming H_2O, instead of H_2O_2. In this sense, one needs to consider some essentially relevant properties of the cathode material, such as high surface area and porosity, nanostructure and particle size, active sites containing oxygenated functional groups and large potential range [8,12,16].

A number of studies published in the literature have often reported the use of carbon-based materials as cathodic matrix with high efficiency for H_2O_2 electrogeneration [14–17], such as reticulated vitreous carbon (RVC) [18,19], graphite felt [19,20], graphite (GRA) [21], carbon nanotubes (CNT) [21,22] and amorphous carbon black (CB) [12,16,23–25,47]. According to Yeager E. (1984), the oxygenated groups present on the surface of carbon-based materials are strictly related to the adsorption energy of molecular O_2, and consequently, to ORR [17].

Reticulated vitreous carbon (RVC) is a widely used cathode material for H_2O_2 electrogeneration. This material has chemical stability in acidic or basic medium; and it can also be applied in flow-through electrodes, increasing the electrode surface area for O_2 reduction and H_2O_2 electrogeneration [18]. Graphite is another carbon-based material that presents good characteristics as an electrode material; this material is known for its relative chemical stability, good electrical conductivity, apart from being relatively cheap. However, graphite is found to be relatively less capable of increasing the electrode surface area. Some studies have reported other forms of graphite application in electrochemical systems; among these diverse applications of graphite includes its use as a helpful support for potentializing H_2O_2 electrogeneration [20,21].

Printex L6 carbon (PL6C) is an amorphous carbon black (CB) with particle size of about 15–18 nm and surface area of 265 $m^2 g^{-1}$ [15] . Recent studies have shown that PL6C is a great cathodic material for H_2O_2 electrogeneration. Assumpção *et al.* (2011) have shown that PL6C presents relatively higher current efficiency compared to Vulcan XC-72R carbon (another type of amorphous CB), with the former contributing toward an improvement of 37% in ORR efficiency for H_2O_2 electrogeneration. These researchers have also demonstrated that high surface area, hydrophilicity, and high content of oxygenated functional groups are key factors when it comes to increasing H_2O_2 electrogeneration [16]. Printex XE2B (PXE2BC) carbon is another type of amorphous carbon black with high amounts of oxygenated functional groups and high surface area. However, very few studies published in the literature have reported the use of this material as a catalyst for ORR.

Some studies have employed carbon-based materials as cathodes in H_2O_2 electrogeneration; unfortunately, these materials were found to have been mostly derived from petroleum, which is a non-renewable natural resource [21–25]. The materials were obtained from incomplete combustion of petroleum-based compounds, and have been found to contribute toward environmental degradation, including toxic gas production, increased acid rain, and greenhouse effect.

Other related studies have reported the use of the biomass of lignin, chitosan, cellulose, and melanin as low-cost carbon-based materials from renewable sources [26–28]. Biomass is an excellent source of sustainable energy, which is known to be environmentally harmless; it can be used as a substitute to carbon derived from non-renewable sources. Lignin is one of the most abundant natural polymers and an important source of biomass; it accounts for nearly 30% of wood weight. One needs to point out, however, that carbon derived from biomass burning has low conductivity and ORR activity. These shortcomings can be circumvented through an activation process, which will provide the carbon material with interesting electrochemical properties, such as large surface area, porosity and active functional groups for ORR [26–28].

The existence and development of new carbon-based materials, which are synthesized through different sources (petroleum, natural or renewable), allows one to evaluate them as new matrices for ORR. The study of these materials focusing mainly on their structural and physicochemical properties, such as morphology, surface area, hydrophilicity, and their possession or not of functional groups, will enable one to choose the best catalyst to employ when conducting reduction reactions. In this context, the main objective of this work is to investigate the effects of structural and physicochemical properties of different carbon-based catalysts on oxygen reduction reaction for H_2O_2 electrogeneration. To this end, graphite (GRA), glassy carbon powder (GC), lignin-derived carbon (LIGC) and black carbon Printex L6 (PL6C) and Printex XE2B (PXE2B) were evaluated.

2. Experimental

2.1. Reagents and materials

Glassy carbon powder and Graphite HC30 were obtained from Goodfellow and Nacional do Grafite Ltda, respectively. Both Printex L6 and Printex XE2B carbon, were acquired from Evonik do Brasil Ltda. Carbon derived from lignin (LIGC) was synthesized based on a previously reported procedure [26,27]. All chemicals employed in the experiments were of reagent grade, and were used without further purification.

2.2. Preparation of carbon micro layer

The carbon materials were evaluated from the manufacture of carbon micro layers deposited on glassy carbon electrodes. Prior to the deposition of the micro layers, the glassy carbon electrodes were polished with alumina (0.3 μm) in a polishing cloth. Subsequently, the electrodes were sonicated for 5 min in isopropanol

and ultrapure water. Carbon dispersions were prepared using a mixture of 2.5 mg of carbon material with 1.0 mL of dimethylformamide (DMF) for glassy carbon 0.4–12 μm (GC), lignin-derived carbon (LIGC), graphite (GRA) and Printex L6 carbon (PL6C). DMF/Water (70/30) was used for the preparation of Printex XE2B carbon (PXE2BC) dispersion. The micro layers were prepared using 10 μL and 25 μL droplets of the carbon suspensions on the GCE surface in order to perform EIS and ORR measurements, respectively; this was followed by the evaporation of the solvent with N_2 flow.

2.3. Characterization techniques

Morphological characterization of the carbon materials was carried out using a field emission gun scanning electron microscope (FEG-SEM), Jeol JSM 7500F model. Contact angle analyses for the carbon materials were conducted with the aid of an Attension Theta Flex tensiometer. An amount of 3.0 μL of ultrapure water was dripped onto the carbon micro layers surface, and the contact angle measurements were performed. BET measurements were conducted by nitrogen physisorption using Micromeritics Gemini VII equipment. The surface area of the samples was calculated using the Brunauer-Emmett-Teller (BET) method for a region of P/P0 0.3.

Raman spectroscopy analyses were performed using Witec model Alpha 300R spectrometer equipped with an argon-ion laser of 514 nm, operated at low power level. The spectra were obtained in the wavenumbers ranging from 0 to 4000 cm^{-1}. XPS analysis of the carbon samples was performed by K-Alpha X-ray photoelectron spectrometer from Thermo Scientific. The Al Kalpha line was employed, and the energy step size was set to 0.1 eV. The background of the C1s and O1s electron spectra was determined.

Electrochemical impedance spectroscopy (EIS) was conducted at open circuit potential. The measurements were performed in an electrochemical cell with a capacity of 10 mL and composed of three electrodes. Bare and modified glassy carbon electrodes (∅ = 5 mm) were used as working electrode. The reference electrode was Ag/AgCl (KCl 3.0 mol L^{-1}) and platinum plate was used as auxiliary electrode. Cyclic voltammetry (CV) measurements were carried out in a potential range of −0.2 to + 0.8 V, at scan rate of 50 mV s^{-1}. EIS experiments were performed in a solution containing 2.0 mmol L^{-1} $K_4[Fe(CN)_6]$ and 0.1 mol L^{-1} KCl. The frequency range of 100 kHz to 100 MHz and 10 mV of amplitude were employed.

2.4. Oxygen reduction reaction analysis

Electrochemical experiments were performed using Potenciostat/Galvanostat Autolab PGSTAT-128 N controlled by NOVA software for data acquisition. ORR analysis was carried out in a devised three-electrode cell using a RRDE (from Pine Instruments – AFE7R9GCPT) as working electrode, Ag/AgCl as reference electrode (KCl 3.0 mol L^{-1}) and a Pt counter electrode. Cyclic voltammetry was performed in a potential window of + 1.0 to −0.8 V at 50 mV s^{-1} in 0.1 mol L^{-1} K_2SO_4 at pH 2.5 adjusted with H_2SO_4, and saturated with N_2 or O_2. Linear sweep voltammetry (LSV) measurements were performed on the same electrolyte and saturated with O_2 only. The potential window of + 0.4 to −0.8 V was applied to the RRDE disk; and a fixed constant potential of + 1.0 V was applied to the ring. The electrode rotation applied was 900 rpm.

3. Results and discussion

3.1. Morphological and structural characterization

The morphology of the carbon materials is illustrated in Fig. 1. The FEG-SEM image of GC shows spheres with sizes ranging from 0.5 to 12 μm (Fig. 1A); the estimated sizes of the spheres are in accordance with those reported by the manufacturer (0.4–12 μm). The glassy carbon spheres were found to be dense and apparently smooth. Due to the different sizes, vacancies were formed between the GC spheres on the film deposited on the substrate.

Fig. 1B shows LIGC exhibiting a heterogeneous structure, where one can observe the formation of plates coated with particles of different sizes forming clusters. The morphology of LIGC may be directly related to its synthesis and the raw material. The morphology of Lignin is similar to that of LIGC; it is characterized by the formation of globules and agglomerated particles which are referred to as “bunch of grapes” structure [28].

Fig. 1C shows the image of the characteristic structure of the sheet-shaped GRA. In the absence of chemical treatment for the exfoliation of this material, graphite sheets will usually be found agglomerated and distributed in piles [29].

PCL6C and PXE2BC have similar morphology (see Fig. 1D and 1E, respectively), and are both referred to as carbon black. Both PCL6C and PXE2BC can be found evenly distributed on the substrate, and have much smaller particles compared to the other carbon materials (about 20 nm in diameter). Another feature of the Printex carbon films is their porosity, which is attributed to the vacancies formed by the agglomeration of carbon particles (see the insets of Fig. 1D and 1E).

The physical structure of the material (its surface area, for instance) is regarded essentially relevant in that it can contribute toward improving ORR electrocatalytic activity, leading to H_2O_2 electrogeneration. Surface area is directly related to the number of ORR active sites; this implies that by increasing the surface area, the number of active sites will also be increased, thus raising the number of free active sites available for ORR to occur. Taking that into consideration, Brunauer-Emmett-Teller (BET) analyses were performed in order to find the surface area value of each carbon material (see Table 1).

Based on BET analyses, the surface area of GRA was found to be about 20.9 m^2 g^{-1}; this was the lowest surface area value among the carbon materials investigated. BET surface area values for LIGC, PL6C and GC were 248.9, 263.8 and 286.1 m^2 g^{-1}, respectively. PXE2BC presented BET surface area of 1028.2 m^2 g^{-1}; the highest among the carbon materials. The surface area values for PL6C and PXE2BC obtained in this work are very close to those reported in the literature/by the manufacturer (265 and 1000 m^2 g^{-1}, respectively) [15,29]. LIGC BET surface area as reported in the literature or by the manufacturer varies from 90 to 880 m^2 g^{-1} [26,27].

By analyzing the BET results obtained for the carbon materials, one will infer that the fact that PXE2BC presented the highest surface area means it will probably have the highest catalytic activity for ORR, followed by the intermediate values and the lower values, in this order. However, it is worth pointing out that in addition to the surface area, ORR catalytic activity is also strongly dependent on the types of functional groups present in the material.

According to Yeager [14], carbon-based material or graphite can generate hydrogen peroxide through the interaction between O_2 species with carbons neighboring the functional group present on its surface. The difference in electronegativity between the functional groups and the neighboring carbon atom may alter the electron distribution of this adjacent C by the displacement of electrons π, affecting its physical and chemical properties. This way, the functional group acts by removing or donating electron density of this carbon (ORR active site) and, consequently, exerting influence over the O_2 adsorption energy with the formation of •OOH intermediate species (Eqs. (4) and (5)). These changes in the active site and, consequently, in the interaction with O_2 may alter the formation of the final product (H_2O or H_2O_2) (see Fig. 2A).

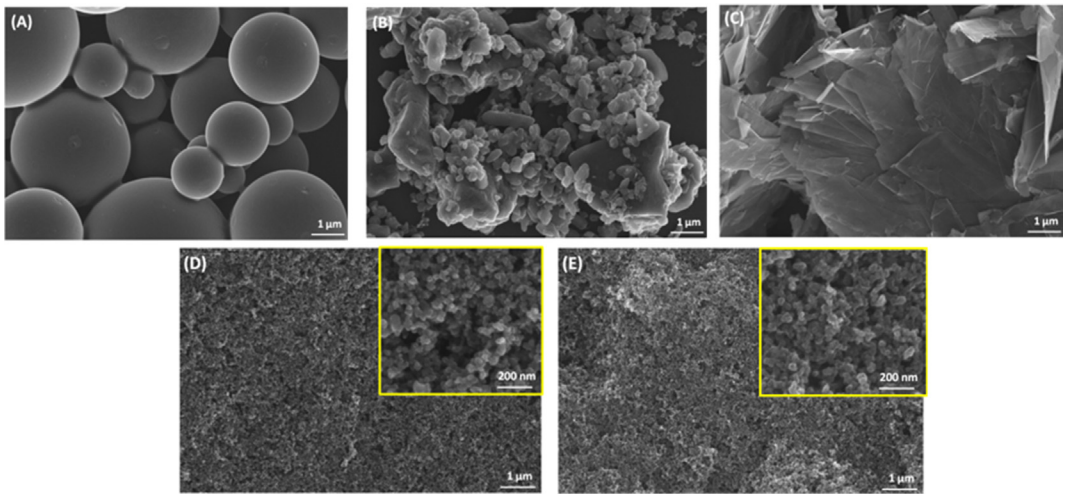

Fig. 1. FEG-SEM images of the carbon samples: GC (A), LIGC (B), GRA (C), PL6C (D) e PXE2BC (E).

Table 1
Estimates of surface area and element contents for GC, LIGC, GRA, PL6C and PXE2BC obtained by elemental analysis.

Material	Area BET ($m^2\ g^{-1}$)	%C	%H	%O	%N	%S
GC	286.1	76.1	0.3	23.3	0.3	*
LIGC	248.9	82.4	0.6	16.7	0.3	*
GRA	20.9	> 99	*	*	*	*
PL6C	263.8	86.7	0.2	12.9	0.1	0,1
PXE2BC	1028.2	83.7	0.4	15.7	0.2	*

* Undiscovered values

In an ideal interaction energy, the •OOH species promotes the electrogeneration of H_2O_2 via $2e^-$ ORR pathway (Eq. (6)). When this interaction is strong, the •OOH residence time will be long enough for the formation of HO* species, leading to H_2O generation via 2 more electrons (Equations (7) and (8)).

$$O_{2(g)} + * \rightarrow O_2* \quad (4)$$

$$O_2* + H^+_{(aq)} + e^- \rightarrow HOO* \quad (5)$$

$$HOO* + H^+_{(aq)} + e^- \rightarrow H_2O_2* \quad (6)$$

$$HOO* \rightarrow O* + HO* \quad (7)$$

$$HO* + H^+_{(aq)} + e^- \rightarrow H_2O* \quad (8)$$

Here, the use of the symbol * shows that the species are adsorbed on the active site. To put it briefly, the type of functional group can play an influential role on the adsorption energy of O_2 and, consequently, on which pathway ORR will occur. According to Ma [30], O-containing functional groups, such as —COOH, —CHO, —C═O, —C—O—C and —COH, present in significant amounts on the amorphous carbon surface, may participate in ORR reactions. In addition, N-containing functional groups, including N-pyridine, N-pyrrolic, N-quaternary and N-oxides, are also found to have catalytic effects on ORR (Fig. 2B).

XPS (Fig. 3) and Raman (Fig. 4) analyses were performed in order to evaluate the influence of the functional groups present in each material. In addition, as aforementioned, elemental analysis was conducted in order to determine the atomic percentage (at. %) content of each element (C, H, O, N, Na and S) present in the carbon materials investigated (see Table S1). Based on the results obtained in the elemental analysis, except for graphite, all the carbon materials investigated presented high levels of C as the major element (92.2 to 99.0 at. %), with O being the second highest one (1.0 to 4.6 at. %). These results indicate the presence of oxygen functional groups (C—O, C═O or O—C═O). The GC sample was found to possess nitrogen functional groups in their structure, since N levels were detected (0.2 at.%). Into PXE2BC sample there was no S or N, but Na was detected with a 2.7 at.%.

XPS analysis was performed for all the carbon-based materials aiming at confirming the presence of functional groups in these materials. The binding structure was determined by the deconvolution of C chemical shifts (C1s spectra) – see Fig. 3 and Table S1. Survey analysis is a useful tool to study the C based materials surface and near-surface region. First information can be obtained from the surface elemental composition, where basal graphite surface should only contain carbon on its structure. Table S1 shows survey data for all analyzed samples, where it is possible to observe a carbon-based material surface with very few defects being able to find sulfur (S2p) with 0.2 at.% for GRA sample, nitrate (N1s) with 0.2 at.% of for GC sample in a very small amount. The only exception was the PXE2BC sample, with high sodium concentration (2.7 at.%). For samples LIGC and PL6C only carbon and oxygen were found.

The C1s spectra were fitted, and carbonyl bonds (C—C) peak was 284.5 eV which is related to graphitic carbon. The GC sample showed to be with higher percentage area (53.9%) FWHM of 1.08 eV when compared to all analyzed samples, while the PXE2BC samples showed the lowest area (39.1%) and the GRA samples showed the lowest FWHM with value of 0.72 eV. Also, GRA sample was the only one to exhibit the high binding energy component located at 289 eV; this peak is typically associated with $\pi \rightarrow \pi^*$ transitions (24.1%). An interesting point worth mentioning is the intensity of the aromatic C-C component, which measures the degree of carbon aromaticity. Compared to the other carbon-based materials, GRA possesses a relatively higher intensity C—C peak (Table 2 and Fig. 3), exhibiting a high degree of carbon with sp2 hybridization [13,16].

The C-H contribution is attributed to aliphatic hydrocarbons; were the C hybrid state is mostly located at sp3 peaks and its area varieties of a range of 28.4–36.7 %, also, no contribution of sp3 peaks into GC samples was observed. The C═O oxygenated functional group is located at 290 eV and was found in both GC and LIGC samples (10.4 and 25.0%, respectively), while the oxygenated

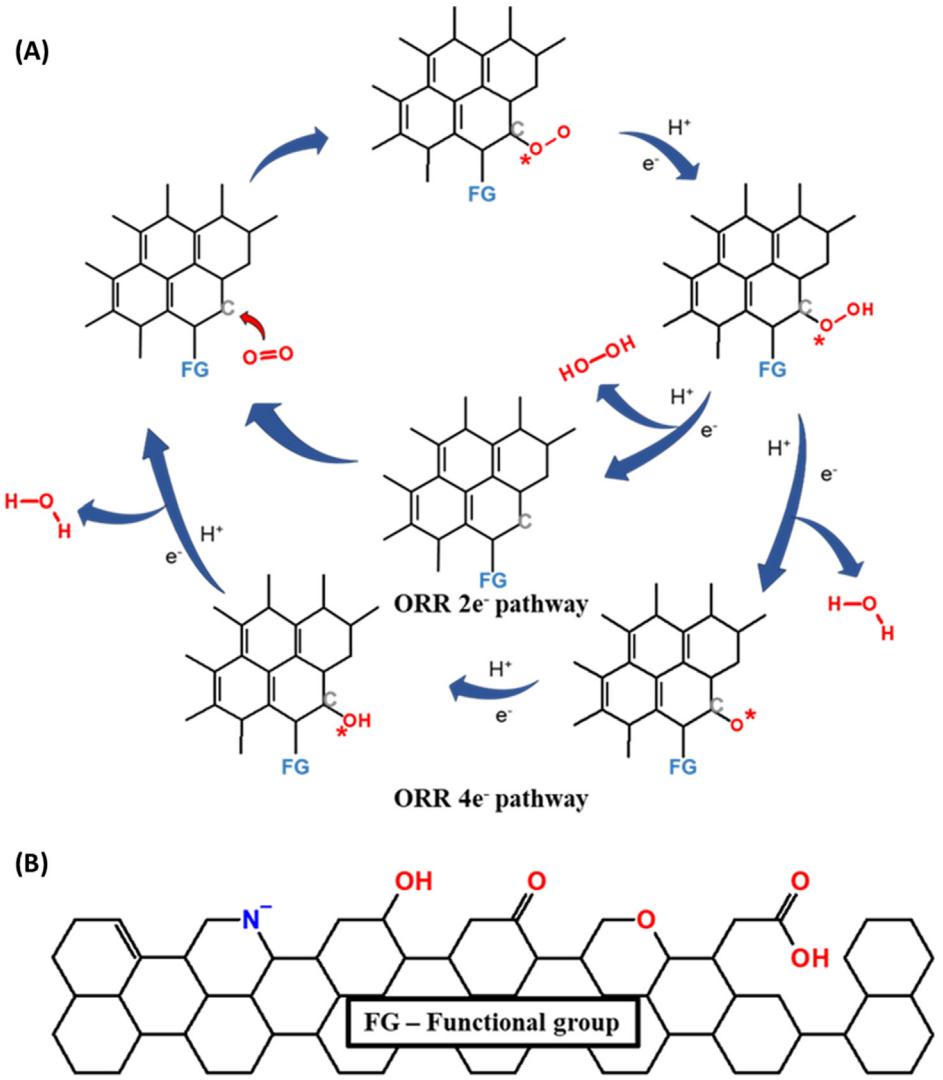

Fig. 2. (a) Scheme of the two possible ORR pathways showing the mechanisms of O_2 molecule adsorption on the active site neighboring the functional group (FG), and (b) some types of functional groups present in the structure of carbon-based materials.

functional group at 286 eV (C—O—C) was found in the GC material only with an area of 35.7%. The PL6C and XE2BC samples presented a similar C1s spectra with aromatic C—C and C—H sub-peak, which are related to graphitic carbon and aliphatic hydrocarbons, respectively. The carboxylic group (O—C=O) located at 288.5 eV with areas of 18.6% and 28.9% respectively, was attributed to the oxygenated functional group present in the structure of PL6C and XE2BC materials.

Since the FWHM value depends on the heterogeneity of the electronic environment of the carbon atoms on the surface material, analyzing the C1s peaks (C-C), makes possible to conclude that the higher values attributed to FWHM of all samples studied the lowest it is the graphitic character of its surface [31]. The sample with the highest conductivity should also had the smallest FWHM, in this case the GRA samples shows the best potential application with 0.72 eV, GRA. The LIGC and PXE2BC shows intermediate FWHM values (0.94 and 0.91 eV) while GC and PL6C samples shows the highest ones (1.08 and 0.97 eV). The fitted O1s core-level spectra are similar for all analyzed samples and are located at 532.5 eV related to C=O group.

Fig. 4 shows the high-resolution spectra of all analyzed samples from the fermi energy edge up to 60 eV. It is possible to note that the C2p peaks related to C2p-π/C2p-σ bands do not appear, and only for LIGC sample the O2s-C2s peak is present. Fig. 4 illustrate the region where those peaks should appear at the spectra [32]. In Fig. 4c, it can be observed the valence band maximum (VBM) of all analyzed samples, where a shift of O2p can be clearly observed at −2.0 up to −6.0 eV. The VBM is predominantly composed of O2p states, while the conduction band minimum (CBM) is composed of C2p states also showed a peak shift clearly observed at −5.0 up to −10.0 eV. The charge carrier migration that occurs into analyzed materials interfaces, indicates that the photo-generated electrons generated at O2p orbitals transfer to carbon C2p orbitals, leaving the photo-generated holes in O2p orbitals, making the material suitable for separation of photo-generated electron–hole pairs [33,34].

Raman spectroscopy analysis was carried out in order to confirm the aromaticity degree of the samples (see Fig. 5). The Raman spectra of all the amorphous carbon samples exhibited two characteristic bands: the D band at 1350 cm^{-1} and the G band ranging from 1580 to 1600 cm^{-1}. These bands are responsible of the different optical, electronic and mechanical properties of the materials according to the ratio of both bands. The D band is related to sp3 bonds, and as such, indicates carbon disorder and imperfections. The G band is associated with sp2-bonded vibration of graphene or unique graphite crystal. GRA presents a D-peak at 1360 cm^{-1}

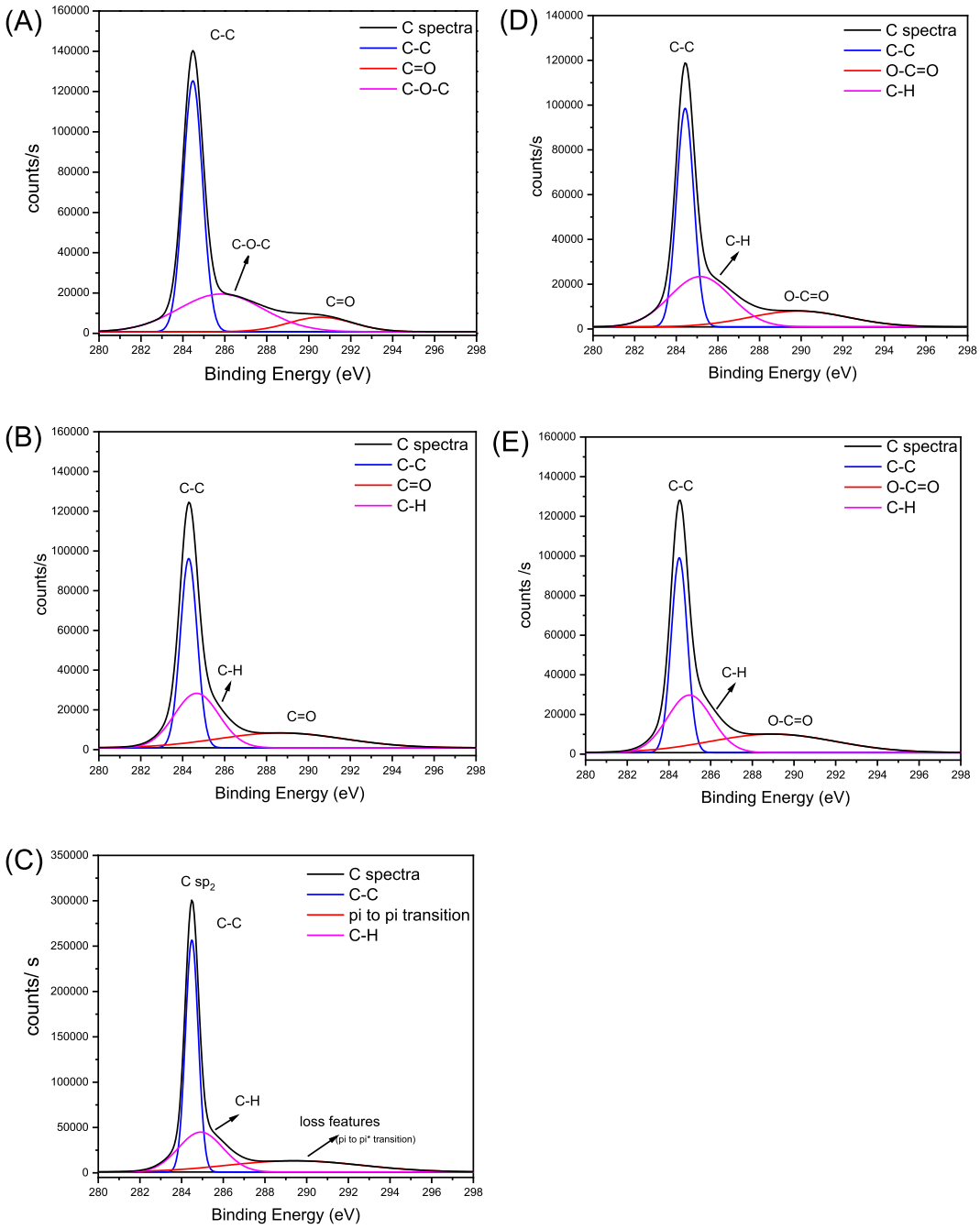

Fig. 3. C1s XPS spectra for GC (A), LIGC (B), GRA (C), PL6C (D), PXE2BC (E).

and a high intensity G peak at 1590 cm^{-1}; this indicates that GRA possesses higher sp2 [35–38].

The PL6C, PXE2BC, LIGC and GC carbon materials showed the G-peak displaced to values close to 1600 cm^{-1}; and an increase was observed in the peak intensity of D-band. This behavior is attributed to the increase in carbon disorder and imperfections, which characterizes samples that are in transition from nanocrystalline graphite to amorphous carbon. The disorder or interference in the structure of carbon materials may be related to the presence of oxygenated functional groups or edge carbon, which are found to enhance ORR catalytic activity, promoting higher H_2O_2 generation [35–38].

The I_D/I_G ratio was calculated in order to evaluate the degree of order/disorder of the amorphous carbon materials. GRA presented a low I_D/I_G; this implies a greater degree of purity and a decrease in the number of defective sites. The other carbon samples presented higher I_D/I_G ratio in the following order: LIG < GC < PL6C < PXE2BC.

The I_D/I_G values show the similar sp2/sp3 ratio between LIGC and GC (1.6), as for PL6C and PXE2BC (1.8), which is only different for GRA (0.2) material. The correlation between the disorder degree of the material and its efficiency for the H_2O_2 production is not clear, however these data show some characteristics to understand the action of the materials in the ORR.

The degree of intermediate disorder for LIGC and GC shows a behavior of materials in transition from graphical to amorphous structures. The greater degree of disorder implies more oxygenated functional groups and more carbon edges are found in the material structure. The PL6C and PXE2BC materials were the ones with the

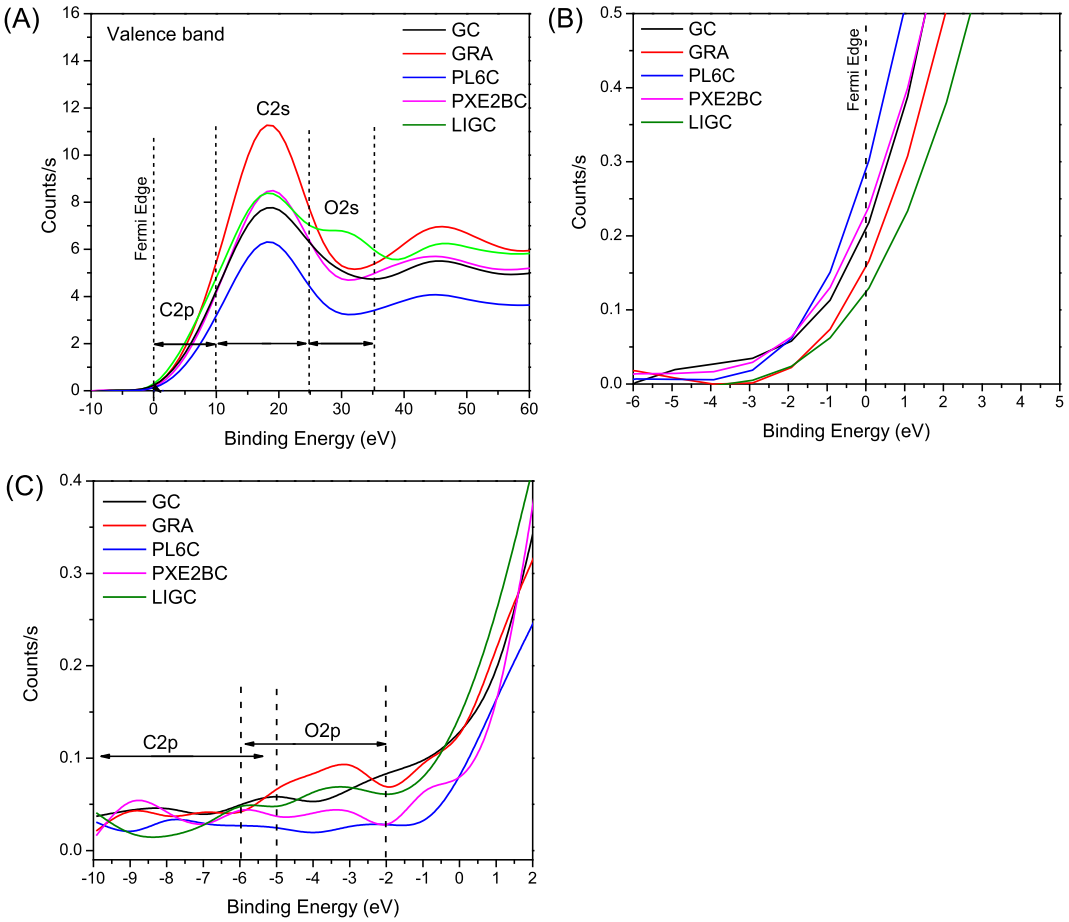

Fig. 4. High-resolution valence band (VB) spectra with intensity ratios of C2p, C2s and O2s peak-maxima (A). The lines shown in (A) are guides to the eye only. Enlarged view of VB spectra at the vicinity of Fermi level (B). Spectra with intensity ratios of C2p and O2p (C). The lines shown in (A) and (C) are guides to the eye only.

Table 2
Carbon XPS spectra, relative peak areas and FWHM of the C1 peaks.

Sample	Area of C 1 s peaks (%)						FWHM C1 peak (eV)
	C—C	C—H	C═O	C—O—C	O—C═O	π - π*	
GC	53.9	–	10.4	35.7	–	–	1.08
LIGC	42.5	32.5	25.0	–	–	–	0.94
GRA	47.5	28.4	–	–	–	24.1	0.72
PL6C	44.7	36.7	–	–	18.6	–	0.97
PXE2BC	39.1	31.9	–	–	28.9	–	0.91

highest degree of disorder, with the highest amorphous structure, high oxidation status (oxygenated functional groups) and edges carbon on the structure. Finally, the GRA showed a lower degree of disorder with a greater sp2 characteristic in a graphical structure. According to these results, this material has a low amount of amorphous structure, with few defects and an unspecified presence of oxygenated functional groups. However, an expressive feature in GRA towards ORR activity is the presence of a laminar structure with the massive composition of C═C sp2 bond, also activators of ORR.

The amount of oxygenated functional groups can influence the hydrophilic surface of the materials. As reported in the literature [13,16], carbon materials with high concentration of oxygenated functional groups are found to be more hydrophilic; and this enhances ORR catalytic activity via $2e^-$. In addition, the presence of oxygenated functional groups and aliphatic groups on the carbon surface allows the formation of hydrogen bonds with the water from the solution. This leads to an increase in the hydrophilic character of the material, which, in turn, contributes to the catalytic activity of ORR, improving the production of H_2O_2 [13,16].

Contact angle assays were performed in order to evaluate the degree of hydrophilicity of the materials (see Fig. 6). The results obtained clearly show that the chemical composition of the samples strongly affect their contact angle with water. The following trend was observed based on the results: θGRA > θPL6C > θPXE2BC > θLIGC > θGC. The results imply that the samples have different degrees of hydrophilicity (and, hence, wettability). The higher the contact angle, the lower the hydrophilicity of the material. GRA was found to have the lowest degree of hydrophilicity among the samples. GC presented the highest degree of hydrophilicity and wettability. Pouring droplets of water on the GRA sample did not make it wet (contact angle

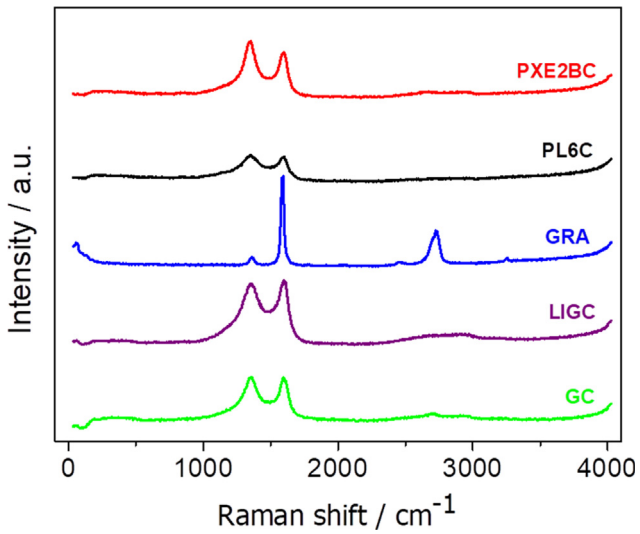

Fig. 5. Raman spectra of GC, LIGC, GRA, PL6C and PXE2BC materials.

135°); by contrast, the GC and LIGC samples (contact angle 15.4° and 20.1°, respectively) became wet when water was poured on the surface. PL6C and PXE2BC were found lying in-between those two extremes, with PL6C presenting a slightly higher degree of wettability (contact angle 63.7°) than PXE2BC (contact angle 41.2°). Furthermore, the shape and size of the water droplets were not found to produce any significant variation during the measurement time; this indicates that the surface forces were in equilibrium.

3.2. Electrochemical characterization

For the analysis of the electrochemical behavior and the charge transfer resistance of the different carbon materials, CV and EIS experiments were performed in 2.0 mmol L^{-1} $K_4[Fe(CN)_6]$ and 0.1 mol L^{-1} KCl. Fig. 7A shows the cyclic voltammograms obtained for the GC, LIGC, GRA, PL6C and PXE2BC materials. It could be seen that redox pair peaks of $K_4[Fe(CN)_6]$ are much more defined and reversible at LIGC, GRA, PL6C and PXE2BC compared to GC material. The electrochemical response of the GC spheres with the $K_4[Fe(CN)_6]$ probe shows greater peak-to-peak separation (ΔE_p) and lower current, and this is due to the limitation of the electron transfer rate, in this material in addition to its relatively lower active area, as shown in BET measures.

Looking at the voltammograms of LIGC, GRA, PL6C (see Fig. 7A), one can observe almost reversible oxi-reduction processes in these materials. However, a slight increase is observed in potassium ferricyanide redox peak currents in the following order: LIGC > GRA and GRA > PL6C; this shows that PL6C is more electroative than LIGC and GRA. In comparison with the PL6C, the PXE2BC voltammogram did not show displacement of $K_4[Fe(CN)_6]$ redox potentials to less positive values. However, the PXE2BC material showed an increase in the capacitive and fararic currents of the cyclic voltammogram. This behavior is found to be typical of materials with high surface area, as observed in the BET analysis. With the subtraction of the capacitive current, the faradic current of this material is in the same order of magnitude as the other carbon materials (except for the GC), showing that for the $K_4[Fe(CN)_6]$ mediator redox reaction studied, the LIG, GRA, PL6C and PXE2BC materials showed similar electrocatalytic effects on CV measurements.

EIS was performed in order to study the interface of carbon materials and their conductivity. The nyquist spectra and equivalent circuit used for the study of the materials interface are shown in Fig. 7B, where the circuit is composed of solution resistance (R_{sol}), charge transfer resistance (R_{ct}), Warburg impedance (W) and capacitance of the double electric layer (C_{dl}).

The Rct value calculated based on the equivalent circuit for the carbon materials investigated are presented in Table 3.

GC presented the lowest conductivity, followed by LIGC, GRA, PL6C and PXE2BC. The high charge transfer resistance of GC may

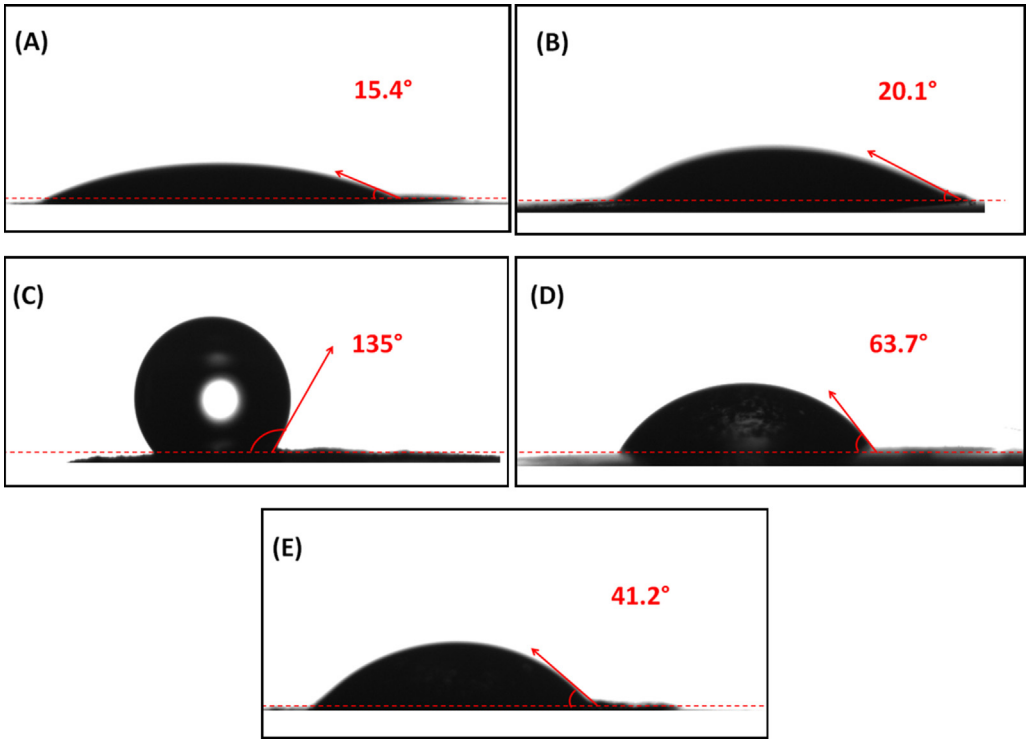

Fig. 6. Pictures and contact angle measurements of 3 μL ultrapure water dropped on micro layers of GC (A), LIGC (B), GRA (C), PL6C (D) e PXE2BC (E).

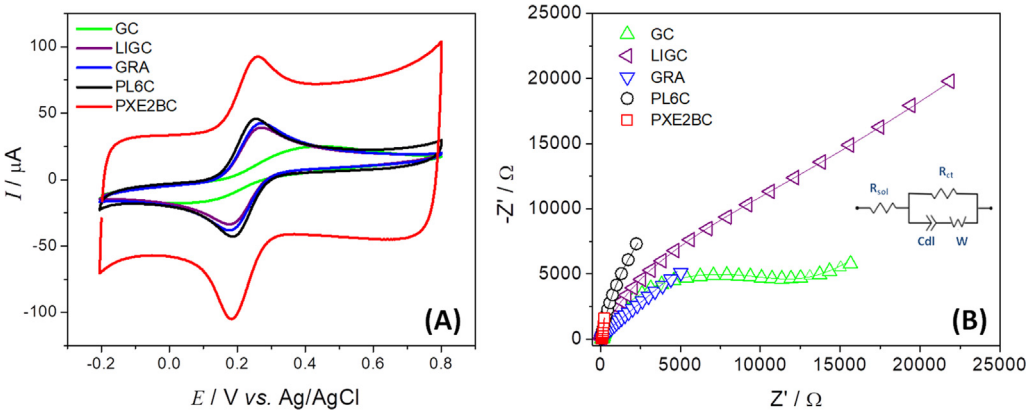

Fig. 7. (A) CV and (B) nyquist spectra of GC, LIGC, GRA, PL6C and PXE2BC materials.

Table 3
Charge transfer resistance (Rct) of carbon materials.

Carbon material	GC	LIGC	GRA	PL6C	PXE2BC
Rct (Ω)	11,652	9459.3	6446.2	4208.8	166.60

be associated with its lower surface area compared to other carbon materials. The presence of functional groups associated with a large surface area boosts electrons transfer, leading to an increase in the conductivity of the material. PXE2BC was the most conductive carbon material, with a R_{ct} nearly 10-fold lower than LIGC, GRA and PL6C and about 100-fold lower than GC. This material, in addition to having the largest surface area compared to other carbon materials, also has oxygenated functional groups in its structure that facilitate electronic transfer.

The electrochemically active surface area (ECSA) for each carbon material was estimated from the electrochemical capacitance of the double layer of the catalytic surface (Cdl) [39,40]. Electrochemical capacitance was obtained by cyclic voltammetry (CV) in the non-Faradic potential region (at −0.350 V vs Ag/AgCl) at different scanning rates (10 to 100 mV s^{-1}). Figure S1 shows the CV profiles of GC, LIGC, GRA, PL6C and PXE2B CVs at the different scan rates studied. From the linear slope of Fig. 8A, corresponding to Cdl, the electrochemical area of each carbon material was estimated. The Cdl values of GC, LIGC, GRA, PL6C and PXE2B were 6.74×10^{-5}, 1.93×10^{-4}, 2.39×10^{-4}, 9.89×10^{-4} and 1.20×10^{-3}F cm^{-2}, respectively.

The BET specific surface areas do not correspond to the trends of electrochemical surface areas for the carbon materials, (Fig. 8B). The BET surface values were almost constant for GC, LIGC and PCL6, with GRA and PXE2B having the smallest and largest surface area, respectively. However, from the Cdl values (Fig. 8A), it can be seen that the GC has the smallest electrochemical area, followed by LIGC and GRA. The materials PL6C and PXE2B had an electrochemical surface area almost 20 times greater than the other materials studied based on the Cdl values.

The ECSA is the most suitable measure to evaluate the effect of the surface area, since the determination is carried out in electrolyte instead of gas, as is the case with BET. Although BET is effective in evaluating the physical surface area, the evaluation of the intrinsic electrochemical activity of the material is obtained by ECSA from the quantification of density of active catalytic sites [41]. There are different methods for determining the ECSA of a material, however, double-layer capacitance is generally used to evaluate carbon materials [42,43]. Based on the Cdl values, the ECSA was estimated, according to equation (9):

$$ECSA = \frac{Cdl}{Cs} \tag{9}$$

where *Cs* is the standard flat area of capacitance corresponding to 40 µF cm^{-2} [42,44,45]. The ECSA of the GC, LIGC, GRA, PL6C and PXE2B was approximately 1.68, 4.81, 5.96, 24.71 and 30.1 per ECSA

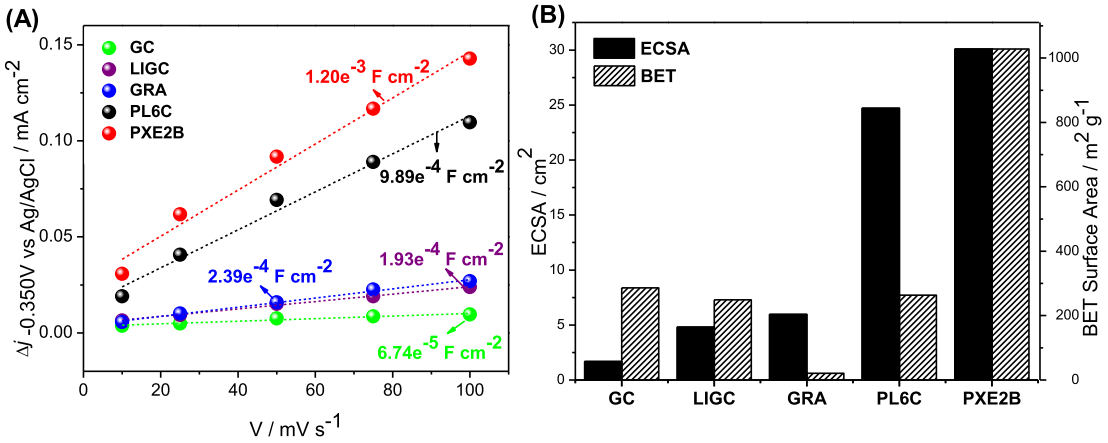

Fig. 8. (A) Capacitive density current average at −0.35 0 V versus the different scan rates; (B) Electrochemical active surface areas (ECSA) and BET surface area for GC, LIGC, GRA, PL6C and PXE2B.

cm^{-2} respectively, Fig. 8B. The morphology, the particle size and the active sites of the carbon materials may have influenced the active electrochemical area of the materials. Structures in the order of μm and form of spheres, sheets or agglomerated plates observed for GC, GRA and LIGC respectively, probably have a smaller contribution to ECSA due to the smaller physical surface area and quantity of active sites and oxygenated functional groups, when compared to PL6C and PXE2B nanoparticles. These results suggest that these printex-type materials have greater electrocatalytic activity.

Fig. 9A and 9B show the cyclic voltammetry (CV) for the micro layer of GC, LIGC, GRA, PL6C and PXE2BC materials in N_2—-and O_2-saturated solutions, respectively. The voltammogram of the N_2-saturated solution (Fig. 9A) shows a redox pair for PXE2BC, PL6C and GRA; this is attributed to the functional groups present in each material. The LIGC and GC materials did not present a faradaic current response in the same potential range; these materials exhibited small or no redox reaction of oxygenated groups (as displayed in the XPS analysis).

PXE2BC and PL6C presented pairs of anode and cathode peaks in the region of −0.2 to −0.4 V (vs. Ag/AgCl), which can be associated with the redox reaction of oxygenated functional groups, such as quinones, anthraquinones, carboxylic acids, found in significant amounts on the surface of these groups. Another relevant observation that merits mentioning is the relatively higher current values obtained for PXE2BC compared to other catalysts (PL6C, in particular). According to the Randles-Sevcik equation, the material area is directly proportional to the current value. Thus, this increase in current value is related to the high surface area of PXE2BC (PXE2BC presented a surface area 3.7 times higher than that of PL6C according to the results obtained from the BET analysis).

Interestingly, although GRA also presented a redox peak in the same potential region investigated, its profile may be associated with the predominance of C=C functional groups, as confirmed by XPS and Raman analyses. The relatively lower current intensity of GRA compared to the Printex carbon materials is attributed to the small surface area and the absence of oxygenated functional groups in GRA.

The CV in O_2-saturated solution (see Fig. 9B) showed the same profile as the N_2-saturated solution, the only exception being the addition of an irreversible ORR peak. The peak potential value

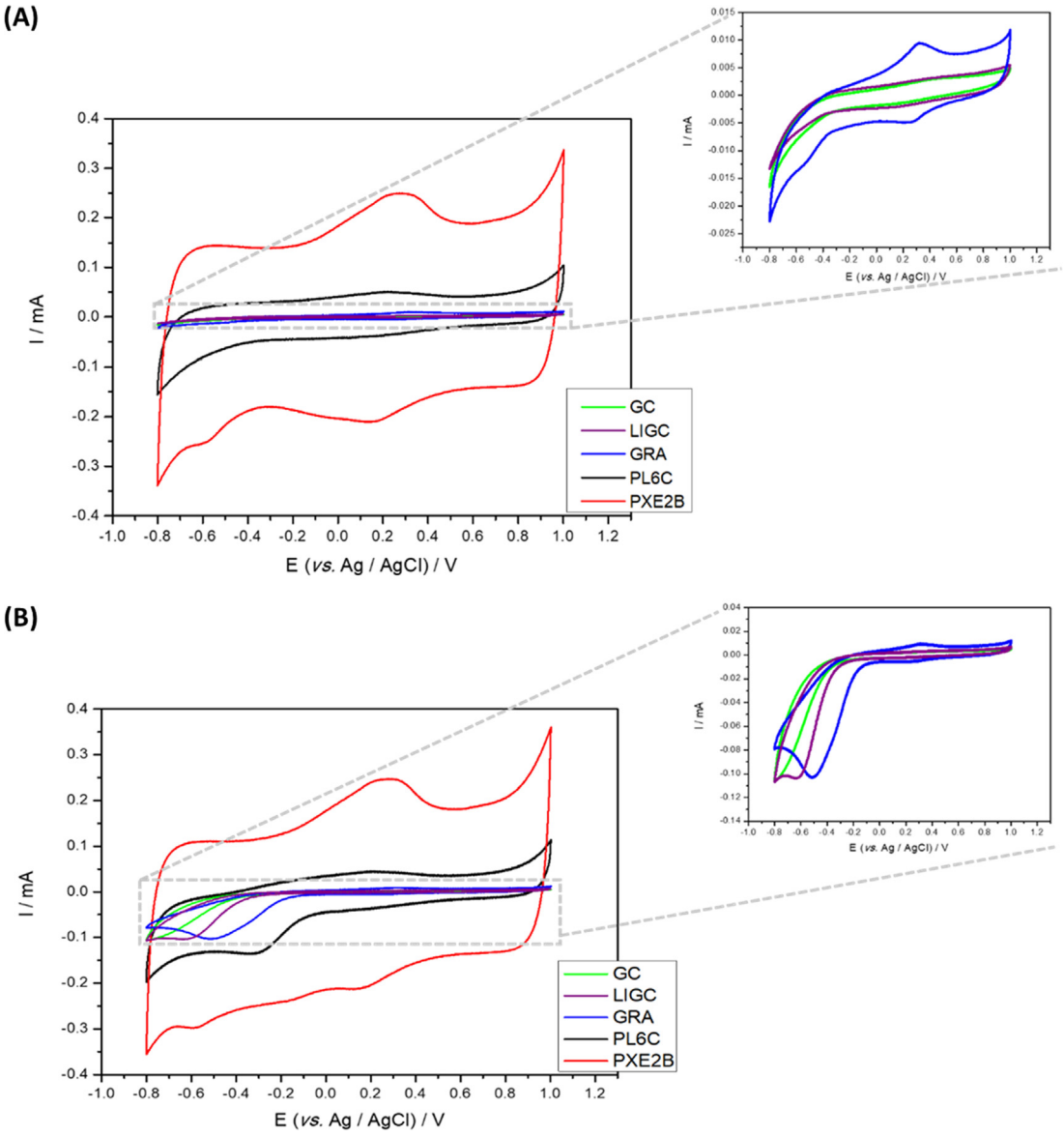

Fig. 9. Cyclic voltammetry curves for GC, LIGC, GRA, PL6C and PXE2BC materials in (A) N_2—-and (B) O_2-saturated electrolyte solution containing 0.1 mol L^{-1} K_2SO_4 (pH = 2,0), at scan rate of 50 mVs^{-1}.

shows the energy required for the reaction to occur; as such, the lower the reaction overpotential applied (values closer to zero), the lower the energy consumption related to the ORR. Of all the carbon materials investigated, GC presented the most negative value for ORR: −0.8 V (vs Ag/AgCl); LIGC and GRA registered the values of −0.6 and −0.5 V, respectively. The Printex carbon samples presented the highest potential shift, with values of −0.3 and −0.2 V (vs. Ag/AgCl) for PL6C and PXE2BC, respectively. Furthermore, with regard to energy consumption in ORR, GC was found to be the material with the highest amount of energy consumption, while PXE2BC consumed the lowest amount of energy.

The shift in the reaction potential can be analyzed in a hydrodynamic process by linear scanning voltammetry with the aid of a rotating ring disk electrode (RRDE). In this experiment, different rotation speeds are generally studied to evaluate the shift in H_2O_2 generation potential and the proportional increase in the current in the disk / ring. This study also makes it possible to assess the physical stability of the carbon micro layer with mechanical agitation, since the increase in rotation leads to a proportional increase in the current, and the opposite behavior may be related to the loss of material on the electrode surface. The LSV obtained for the speeds of 100, 400, 900, 1600 and 2500 rpm are shown in Figure S2, where it is possible to observe a proportional increase of the current with the increase of the rotation. Due to the limited arrival of O_2 on the surface of the micro layer at lower speeds (100 rpm) and its saturation at high speeds (2500 rpm), the rotation speed of 900 rpm was chosen for the discussion of the ORR study.

3.3. ORR study

The study of the ORR of the carbon samples by linear scanning voltammetry was performed using rotating ring-disk electrode (RRDE). The values of currents recorded on the disk are related to the oxygen reduction reaction (ORR). A constant potential was applied on the ring and the current values detected were attributed to H_2O_2 oxidation. Thus, the linear scanning voltammetry graphs obtained had two parts: the upper part, which refers to the current values recorded on the ring, and the bottom part, which is related to the current values recorded on the disk. The correlation between both currents values allows qualitative determination of H_2O_2 efficiency and the number of electrons transferred. To carry out hydrodynamic analysis on the RRDE, the following equations (10 and 11) proposed by Paulus [46] were employed. These equations provide an approximate value of the percentage of H_2O_2 electrogenerated (Eq. (10)), and the number of electrons involved in the reaction (Eq. (11)).

$$H_2O_2\% = \frac{2i_a/N}{i_d + i_a/N}100\% \quad (10)$$

$$n_{e^-} = \frac{i_d}{i_d + \frac{i_a}{N}} \quad (11)$$

where i_d is the current value from the ORR on the disk; i_a is the current value recorded on the ring; and N is the collection number (reported by the RRDE manufacturer - N = 0.37).

In Fig. 10, one can observe that the carbon catalysts present a similar profile, yet the ORR can be found to begin at different potential values. Both GC and LIGC presented potential values close to −0.45 V, with 86.6 ± 1.8% and 88.1 ± 1.4%, respectively, of $\%H_2O_2$ electrogenerated. The percentage value of H_2O_2 electrogenerated means that out of 100% of the reactions that can occur in ORR, the value showed refers to the amount of H_2O_2 generated, while the remainder refers to the amount of H_2O generated. GRA presented an ORR onset shifted towards more positive potentials to −0.30 V, with $\%H_2O_2$ electrogenerated of 92.2 ± 0.8%, followed by PL6C at −0.15 V and PXE2BC close to −0.1 V. The shift of the potential to more positive values suggests lower energy consumption in the ORR process. PL6C and PXE2BC presented 90.3 ± 0.6% and 90.0 ± 0.8%, respectively, of $\%H_2O_2$ electrogenerated.

The number of electrons involved in the ORR process was also determined for the catalysts. The values obtained were close to each other: 2.16 for GRA, 2.19 for PL6C, 2.20 for PXE2BC, 2.24 for LIGC, and 2.26 for GC. The values of $\%H_2O_2$ electrogenerated and the number of electrons can be seen in Fig. 10(B) and (C), respectively. The values presented refer to the average value obtained in the potential range of each material.

In addition to the ORR study, the stability of the films of carbon-based materials was also evaluated, since Nafion was not used in this work. For this, 10 LSV were performed under the same condi-

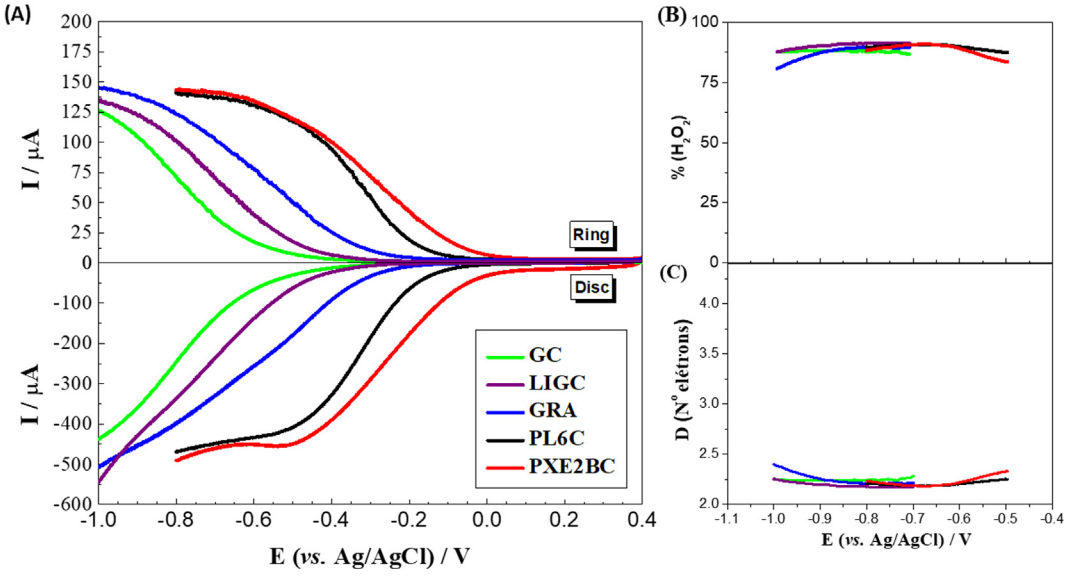

Fig. 10. (A) Linear sweep voltammetry analysis of CG, LICG, GRA, PL6C and PXE2BC; (B) $\%H_2O_2$ electrogenerated and (C) number of electrons involved in the ORR process carried out under the rotation rate of 900 rpm, using a supporting electrolyte containing 0,1 mol L^{-1} of K_2SO_4 (pH 2), in the potential range of 0.4 a − 0.8 V, and at scan rate of 5 mV s^{-1}.

tions as before, and as can be seen in Figure S3, all materials showed high stability, in which the voltammograms overlapped each other.

Therefore, the findings from this study indicate the following order in terms of catalyst efficiency for H_2O_2 electrogeneration: GRA > PL6C > PXE2BC > LIGC > GC. Moreover, high reaction efficiency for obtaining H_2O_2 via $2e^-$ instead of H_2O via $4e^-$ was observed for all materials.

In order of selectivity of the reaction towards H_2O_2 production, the materials presented the following efficiency sequence: PXE2BC > PL6C > GRA > LIGC > GC. Among the carbon-based materials investigated, GC was found to be the least efficient in H_2O_2 electrogeneration probably due to the types of functional groups present in its structure. In line with the results obtained from the XPS analysis, the main functional groups present in the GC material were C—C, C=O and C—O—C; these groups may not have an active participation when it comes to triggering ORR via 2 electrons. The next in line, in terms of poor H_2O_2 electrogeneration, is LIGC, which, with the aid of elemental analysis, showed the presence of nitrogen in larger quantities in relation to the other catalysts. Some researchers suggest that materials with N-functional groups usually target ORR 4-electron pathway. On the other hand, the presence of N-functional groups, such as pyrrolic-N or pyridinic-N within carbon matrices, may contribute to ORR 2-eletron pathway [14,30]; however, these functional groups were not found in the LIGC material investigated in this work. In summary, GC and LIGC showed low activity in the ORR towards H_2O_2 production, due to their low hydrophobicity, low ECSA active area and oxygenated functional groups with low electrochemical activity for the ORR compared to the other carbonaceous materials studied.

The fact that GRA contains C=C groups, the π-π transitions provide electronegative regions which contribute toward increasing the positive charge on the ORR active sites. This facilitates molecular O_2 adsorption compared to C—C (sp3) and non-active functional groups, as observed for GC and LIGC. The presence of C=C sp2 causes a shift in the ORR potential, despite the fact that the carbon material has a small surface area and does not possess oxygen groups on its surface. Its greatest efficiency for H_2O_2 production is related to the laminar structure of material and its low hydrophobicity that facilitates the release of the product via $2e^-$ compared to the porous materials.

The PL6C and PXE2BC catalysts showed the highest electrochemical activity ORR due to the presence of oxygenated functional groups that activate this reaction such as carboxyl (O—C=O) and carbonyl (C=O) and also by hydrophobic characteristics of its surface correlated with its large surface area and high value of active sites.

4. Conclusions

The present work studied the effects of structural and physicochemical properties of different carbon-based catalysts on oxygen reduction reactions. The FEG-SEM results show that morphology and particle size play a significant role on ORR efficiency. Essentially, as observed for the GC, PL6C and PXE2BC catalysts investigated in this study, the smaller the carbon material particles, the higher is its surface area. Among the carbon materials investigated, PXE2BC presented the highest surface area; this is directly related to the number of active sites present on the surface of this material as noted in the ECSA measurement. The high electrochemically active surface area led to the greater displacement of the ORR potential to more positive values; in other words, to lower energy values required for the ORR to occur.

Another factor regarded relevant for the enhancement of ORR efficiency is the type of functional group present in the carbon material. Elemental and XPS analyses have shown that oxygenated functional groups (carboxyl) exert the greatest influence on ORR. These groups facilitate the displacement of the active site electron density and allow a better adsorption interaction of O_2 on the sites, leading to a more efficient electrogeneration of H_2O_2. The GRA showed a small number of oxygenated functional groups, however its activity for the ORR was related to the considerable presence of C=C (Csp2) graphical bonds of the material. Finally, as was observed in the GC and LIGC samples, there may be oxygenated or nitrogenated functional groups that do not have such a positive influence on ORR.

Based on the results obtained in this study, carbon black PXE2BC presented the greatest properties among the carbon materials investigated; the high surface area, quantity and type of oxygenated functional group present in PXE2BC contributed to the highest amount of H_2O_2 electrogeneration via ORR. It is noteworthy that, to date, PXE2BC has been scantly reported in the literature as an ORR electrocatalyst material. The results of this study show that PXE2BC can be used as a suitable catalyst for H_2O_2 electrogeneration by ORR. Further studies need to be carried out in order to better ascertain and explore the properties of this carbon material.

Declaration of Competing Interest

The authors declare that they have no known competing financial interests or personal relationships that could have appeared to influence the work reported in this paper.

Acknowledgements

The authors do acknowledge the financial support provided by the Brazilian research funding agencies, including the Brazilian National Council for Scientific and Technological Development - CNPq (grants no. 465571/2014-0, 301492/2013-1, 302874/2017-8 and 427452/2018-0), São Paulo Research Foundation (FAPESP – grants #2011/14314-1, #2014/50945-4, #2016/19612-4, #2016/01937-4, #2016/08760-2 #2017/10118-0 and #2017/23464-3) and the Coordenação de Aperfeiçoamento de Pessoal de Nível Superior (CAPES – Finance Code 001 and Grant 88887126/2017/00).

Appendix A. Supplementary material

Supplementary data to this article can be found online at https://doi.org/10.1016/j.jcat.2020.09.020.

References

[1] R. Hage, A. Lienke, Applications of transition-metal catalysts to textile and wood-pulp bleaching, Angew. Chem. Int. Ed. 45 (2005) 206–222, https://doi.org/10.1002/anie.200500525.
[2] D. Yu, M. Wu, J. Lin, Establishment of an effective activated peroxide system for low-temperature cotton bleaching using synthesized tetramido macrocyclic iron complex, Fibers Polym. 18 (2017) 1741–1748, https://doi.org/10.1007/s12221-017-7023-0.
[3] G. Blanco-Brieva, M.C. Capel-Sanchez, M.P. De Frutos, A. Padilla-Polo, J.M. Campos-Martin, J.L.G. Fierro, New two-step process for propene oxide production (HPPO) based on the direct synthesis of Hydrogen peroxide, Ind. Eng. Chem. Res. 47 (2008) 8011–8015, https://doi.org/10.1021/ie800245r.
[4] B. Puértolas, A.K. Hill, T. García, B. Solsona, L. Torrente-Murciano, In-situ synthesis of hydrogen peroxide in tandem with selective oxidation reactions: A mini-review, Catal. Today. 248 (2015) 115–127, https://doi.org/10.1016/j.cattod.2014.03.054.
[5] E. Brillas, I. Sire, M.A. Oturan, I. Sirés, M.A. Oturan, Electro-Fenton Process and Related Electrochemical Technologies Based on Fenton ' s Reaction Chemistry, Chem. Rev. 109 (2009) 6570–6631, https://doi.org/10.1021/cr900136g.
[6] M.A. Oturan, J.J. Aaron, Advanced oxidation processes in water/wastewater treatment: Principles and applications. A review, Crit. Rev. Environ. Sci. Technol. 44 (2014) 2577–2641, https://doi.org/10.1080/10643389.2013.829765.
[7] J.R. Kirchner, L.G. Vaughan, United States Patent [19], (1990).

[8] S. Yang, A. Verdaguer-Casadevall, L. Arnarson, L. Silvioli, V. Čolić, R. Frydendal, J. Rossmeisl, I. Chorkendorff, I.E.L. Stephens, Toward the Decentralized Electrochemical Production of H 2 O 2: A Focus on the Catalysis, ACS Catal. 8 (2018) 4064–4081, https://doi.org/10.1021/acscatal.8b00217.
[9] F. Wang, S. Hu, Studies of electrochemical reduction of dioxygen with RRDE, Electrochim. Acta 51 (2006) 4228–4235, https://doi.org/10.1016/j.electacta.2005.11.042.
[10] R.J. Lewis, G.J. Hutchings, Recent Advances in the Direct Synthesis of H 2 O 2, ChemCatChem. 11 (2019) 298–308, https://doi.org/10.1002/cctc.201801435.
[11] H.S. Wroblowa, G. Yen-Chi-Pan, Razumney, Electroreduction of oxygen, J. Electroanal. Chem. Interfacial Electrochem. 69 (2006) 195–201, https://doi.org/10.1016/s0022-0728(76)80250-1.
[12] P.J.M. Cordeiro-Junior, R. Gonçalves, T.T. Guaraldo, R. da Silva Paiva, E.C. Pereira, M.R.de V. Lanza, Oxygen reduction reaction: Semi-empirical quantum mechanical and electrochemical study of Printex L6 carbon black, Carbon N. Y. 156 (2020) 1–9, https://doi.org/10.1016/j.carbon.2019.09.036.
[13] A. Moraes, M.H.M.T. Assumpção, F.C. Simões, V.S. Antonin, M.R.V. Lanza, P. Hammer, M.C. Santos, Surface and Catalytical effects on Treated Carbon Materials for Hydrogen Peroxide Electrogeneration, Electrocatalysis 7 (2016) 60–69, https://doi.org/10.1007/s12678-015-0279-5.
[14] E. Yeager, Dioxygen electrocatalysis: mechanisms in relation to catalyst structure, J. Mol. Catal. 38 (1986) 5–25, https://doi.org/10.1016/0304-5102(86)87045-6.
[15] W. Zhou, X. Meng, J. Gao, A.N. Alshawabkeh, Hydrogen peroxide generation from O 2 electroreduction for environmental remediation: A state-of-the-art review, Chemosphere 225 (2019) 588–607, https://doi.org/10.1016/j.chemosphere.2019.03.042.
[16] M.H.M.T.H.M.T. Assumpção, R.F.B.F.B. De Souza, D.C.C. Rascio, J.C.M.C.M. Silva, M.L.L. Calegaro, I. Gaubeur, T.R.L.C.R.L.C. Paixão, P. Hammer, M.R.V.R.V. Lanza, M.C.C. Santos, A comparative study of the electrogeneration of hydrogen peroxide using Vulcan and Printex carbon supports, Carbon N. Y. 49 (2011) 2842–2851, https://doi.org/10.1016/j.carbon.2011.03.014.
[17] E. Yeager, Electrocatalysts for O_2 reduction, Electrochim. Acta 29 (1984) 1527–1537, https://doi.org/10.1016/0013-4686(84)85006-9.
[18] Q. Li, C. Batchelor-Mcauley, N.S. Lawrence, R.S. Hartshorne, C.J.V. Jones, R.G. Compton, A flow system for hydrogen peroxide production at reticulated vitreous carbon via electroreduction of oxygen, J. Solid State Electrochem. 18 (2014) 1215–1221, https://doi.org/10.1007/s10008-013-2250-9.
[19] J.L. Nava, A. Recéndiz, L.G. González, G. Carreño, F. Martínez, Mass Transport and Potential Studies in a Flow-through Porous Electrode Reactor, Port. Electrochim. Acta. 27 (2009) 381–396, https://doi.org/10.4152/pea.200903381.
[20] Z. Pan, K. Wang, Y. Wang, P. Tsiakaras, S. Song, In-situ electrosynthesis of hydrogen peroxide and wastewater treatment application: A novel strategy for graphite felt activation, Appl. Catal. B Environ. 237 (2018) 392–400, https://doi.org/10.1016/j.apcatb.2018.05.079.
[21] A.R. Khataee, M. Safarpour, M. Zarei, S. Aber, Electrochemical generation of H2O2 using immobilized carbon nanotubes on graphite electrode fed with air: Investigation of operational parameters, J. Electroanal. Chem. 659 (2011) 63–68, https://doi.org/10.1016/j.jelechem.2011.05.002.
[22] R.D.C. Soltani, A. Rezaee, A.R. Khataee, H. Godini, Electrochemical generation of hydrogen peroxide using carbon black-, carbon nanotube-, and carbon black/carbon nanotube-coated gas-diffusion cathodes: Effect of operational parameters and decolorization study, Res. Chem. Intermed. 39 (2013) 4277–4286, https://doi.org/10.1007/s11164-012-0944-8.
[23] P.S. Simas, V.S. Antonin, L.S. Parreira, P. Hammer, F.L. Silva, M.S. Kronka, R.B. Valim, M.R.V. Lanza, M.C. Santos, Carbon Modified with Vanadium Nanoparticles for Hydrogen Peroxide Electrogeneration, Electrocatalysis 8 (2017) 311–320, https://doi.org/10.1007/s12678-017-0366-x.
[24] R.B. Valim, R.M. Reis, P.S. Castro, A.S. Lima, R.S. Rocha, M. Bertotti, M.R.V. Lanza, Electrogeneration of hydrogen peroxide in gas diffusion electrodes modified with tert-butyl-anthraquinone on carbon black support, Carbon N. Y. 61 (2013) 236–244, https://doi.org/10.1016/j.carbon.2013.04.100.
[25] J. Moreira, V. Bocalon Lima, L. Athie Goulart, M.R.V. Lanza, Electrosynthesis of hydrogen peroxide using modified gas diffusion electrodes (MGDE) for environmental applications: Quinones and azo compounds employed as redox modifiers, Appl. Catal. B Environ. 248 (2019) 95–107, https://doi.org/10.1016/j.apcatb.2019.01.071.
[26] W.J. Liu, H. Jiang, H.Q. Yu, Thermochemical conversion of lignin to functional materials: a review and future directions, Green Chem. 17 (2015) 4888–4907, https://doi.org/10.1039/c5gc01054c.
[27] M. Santhiago, P.S. Garcia, M. Strauss, ScienceDirect Bio-based nanostructured carbons toward sustainable technologies, Curr. Opin. Green Sustain. Chem. 12 (2018) 22–26, https://doi.org/10.1016/j.cogsc.2018.04.009.
[28] T.R.R. Brazil, R.N.N. Costa, M. Massi, M.C.C. Rezende, Structural , morphological , and thermal characterization of kraft lignin and its charcoals obtained at different heating rates Structural , morphological , and thermal characterization of kraft lignin and its charcoals obtained at different heating rates, (2018). doi:10.1088/2053-1591/aab7c2.
[29] R. Hack, C.H.G. Correia, R.A.D.S. Zanon, S.H. Pezzin, Characterization of graphene nanosheets obtained by a modified hummer's method, Rev. Mater. 23 (2018), https://doi.org/10.1590/s1517-707620170001.0324.
[30] R. Ma, G. Lin, Y. Zhou, Q. Liu, T. Zhang, A review of oxygen reduction mechanisms for metal-free carbon-based electrocatalysts, Npj Comput. Mater. (2019), https://doi.org/10.1038/s41524-019-0210-3.
[31] D. Pantea, H. Darmstadt, S. Kaliaguine, C. Roy, Electrical conductivity of conductive carbon blacks: Influence of surface chemistry and topology, Appl. Surf. Sci. 217 (2003) 181–193, https://doi.org/10.1016/S0169-4332(03)00550-6.
[32] A. Ganguly, S. Sharma, P. Papakonstantinou, J. Hamilton, Probing the thermal deoxygenation of graphene oxide using high-resolution in situ X-ray-based spectroscopies, J. Phys. Chem. C 115 (2011) 17009–17019, https://doi.org/10.1021/jp203741y.
[33] R. Li, L. Sun, W. Zhan, Y.A. Li, X. Wang, X. Han, Engineering an effective noble-metal-free photocatalyst for hydrogen evolution: Hollow hexagonal porous micro-rods assembled from In2O3@carbon core-shell nanoparticles, J. Mater. Chem. A. 6 (2018) 15747–15754, https://doi.org/10.1039/c8ta04916e.
[34] Z. Azdad, L. Marot, L. Moser, R. Steiner, E. Meyer, Valence band behaviour of zirconium oxide, Photoelectron and Auger spectroscopy study, Sci. Rep. 8 (2018) 1–6, https://doi.org/10.1038/s41598-018-34570-w.
[35] T.T. Guaraldo, L.A. Goulart, F.C. Moraes, M.R.V. Lanza, Carbon black nanospheres modified with Cu (II)-phthalocyanine for electrochemical determination of Trimethoprim antibiotic, Appl. Surf. Sci. 470 (2019) 555–564, https://doi.org/10.1016/j.apsusc.2018.09.226.
[36] F.C. Tai, S.C. Lee, C.H. Wei, S.L. Tyan, Correlation between ID/IG ratio from visible Raman spectra and sp2/sp3 ratio from XPS spectra of annealed hydrogenated DLC film, Mater. Trans. 47 (2006) 1847–1852, https://doi.org/10.2320/matertrans.47.1847.
[37] F.C. Moraes, R.G. Freitas, R. Pereira, L.F. Gorup, A. Cuesta, E.C. Pereira, Coupled electronic and morphologic changes in graphene oxide upon electrochemical reduction, Carbon N. Y. 91 (2015) 11–19, https://doi.org/10.1016/j.carbon.2015.04.038.
[38] A.C. Ferrai, J. Robertson, Interpretation of Raman spectra of disordered and amorphous carbon, Phys. Rev. B. 61 (2000) 14095–14107, https://doi.org/10.1007/BF02543692.
[39] S. Kang, J. Jang, S.H. Ahn, C.S. Lee, Novel design of hollow g-C 3 N 4 nanofibers decorated with MoS 2 and S, N-doped graphene for ternary heterostructures, Dalt. Trans. 48 (2019) 2170–2178, https://doi.org/10.1039/c8dt04656e.
[40] H.L.S. Santos, P.G. Corradini, M. Medina, J.A. Dias, L.H. Mascaro, NiMo-NiCu Inexpensive Composite with High Activity for Hydrogen Evolution Reaction, ACS Appl. Mater. Interf. 12 (2020) 17492–17501, https://doi.org/10.1021/acsami.0c00262.
[41] H. Ren, Y. Pan, C.C. Sorrell, H. Du, Assessment of electrocatalytic activity through the lens of three surface area normalization techniques, J. Mater. Chem. A 8 (2020) 3154–3159, https://doi.org/10.1039/c9ta13170a.
[42] C.C.L. McCrory, S. Jung, J.C. Peters, T.F. Jaramillo, Benchmarking heterogeneous electrocatalysts for the oxygen evolution reaction, J. Am. Chem. Soc. 135 (2013) 16977–16987, https://doi.org/10.1021/ja407115p.
[43] C.R. Zanata, P.S. Fernández, A.B. Santos, G.C. Da Silva, G.A. Camara, C.A. Martins, Estimating the time-dependent performance of nanocatalysts in fuel cells based on a cost-normalization approach, J. Braz. Chem. Soc. 27 (2016) 1980–1988, https://doi.org/10.5935/0103-5053.20160088.
[44] H. Deng, C. Zhang, Y. Xie, T. Tumlin, L. Giri, S.P. Karna, J. Lin, Laser induced MoS2/carbon hybrids for hydrogen evolution reaction catalysts, J. Mater. Chem. A. 4 (2016) 6824–6830, https://doi.org/10.1039/c5ta09322h.
[45] D. Voiry, M. Chhowalla, Y. Gogotsi, N.A. Kotov, Y. Li, R.M. Penner, R.E. Schaak, P. S. Weiss, Best Practices for Reporting Electrocatalytic Performance of Nanomaterials, ACS Nano. 12 (2018) 9635–9638, https://doi.org/10.1021/acsnano.8b07700.
[46] U.A. Paulus, T.J. Schmidt, H.A. Gasteiger, R.J. Behm, Oxygen reduction on a high-surface area Pt / Vulcan carbon catalyst : A thin-film rotating ring-disk electrode study Oxygen reduction on a high-surface area Pt / Vulcan carbon catalyst : a thin-film rotating ring-disk electrode study, Res. Gate. 495 (2014) 134–145, https://doi.org/10.1016/S0022-0728(00)00407-1.
[47] Matheus S. Kronka, Fernando L. Silva, Alysson S. Martins, Michell O. Almeida, Káthia M. Honório, Marcos R.V. Lanza, Tailoring the ORR selectivity for H_2O_2 electrogeneration by modification of Printex L6 carbon with 1,4-naphthoquinone: a theoretical, experimental and environmental application study, Mater. Adv. 1 (5) (2020) 1318–1329, https://doi.org/10.1039/d0ma00290a.